Available online at www.sciencedirect.com

ScienceDirect

journal homepage: http://www.elsevier.com/locate/acme

Original Research Article

Single point incremental forming of Cu-Al composite sheets: A comprehensive study on deformation behaviors

Zhaobing Liu [a,b,c,*], *Guohao Li* [a]

[a] *School of Mechanical and Electronic Engineering, Wuhan University of Technology, Wuhan 430070, China*
[b] *Institute of Advanced Materials and Manufacturing Technology, Wuhan University of Technology, Wuhan 430070, China*
[c] *Hubei Provincial Engineering Technology Research Center for Magnetic Suspension, Wuhan University of Technology, Wuhan 430070, China*

ARTICLE INFO

Article history:
Received 5 July 2018
Accepted 30 November 2018
Available online 4 January 2019

Keywords:
Single point incremental forming
Cu-Al composites
Deformation
Formability
Forming force

ABSTRACT

Compared with monolithic metal sheet, Single Point Incremental Forming (SPIF) of bimetal composite sheet has attracted increasing attention, as it takes advantages of materials with different superior properties, such as high strength, low density, and good corrosion resistance. However, deformation behaviors of bimetal composite sheet in SPIF may differ from the single-layer sheet, which depends on the layer arrangements and mechanical properties of each layer. In this regard, a comprehensive study was conducted to investigate the deformation behaviors of roll-bonded Cu-Al composite sheets in SPIF through predictive modeling, including analytical, empirical as well as numerical approaches, and extensive experimental work taking into consideration effects of key process parameters. It was demonstrated that overall, the formability, surface roughness, thickness variation and forming force in different layer arrangements, in terms of various process parameters, follow the similar trends to single-layer sheets. However, it was further revealed that deformation mode of layer-up sheet tends to a compression state and that of layer-down sheet tends to a stretching state. This leads to higher formability and larger forming force in Al/Cu layer arrangement compared to Cu/Al layer arrangement, as the exterior thinner but stronger Cu layer could endure more stretching deformation.

© 2018 Politechnika Wroclawska. Published by Elsevier B.V. All rights reserved.

1. Introduction

Bimetal composite sheets fabricated by roll bonding have been extensively used in composite structures and components with wide applications in aerospace, electrical, chemical, ship and building industries, as it takes advantages of combined mechanical, physical, and chemical properties from different base materials [1]. Recently, growing interest has been focused on forming processes of bimetal composite sheets by

* *Corresponding author at*: School of Mechanical and Electronic Engineering, Wuhan University of Technology, Wuhan 430070, China.
E-mail address: zhaobingliu@whut.edu.cn (Z. Liu).

https://doi.org/10.1016/j.acme.2018.11.011
1644-9665/© 2018 Politechnika Wroclawska. Published by Elsevier B.V. All rights reserved.

researchers. Traditional forming processes like deep drawing has been considered to process such kind of material. Parsa et al. [2] studied the effects of thickness ratio as well as layer arrangements on the reachable drawing ratio in the deep drawing of aluminum/stainless steel two-layer sheets numerically and experimentally. Results revealed that the aluminum to steel thickness ratio of 1/3 can result in a maximum drawing ratio. Bagherzadeh et al. [3] developed analytical models to perform stress analysis and instability condition in hydro-mechanical deep drawing of Al/Carbon steel sheets. Then, the effect of layer thicknesses, arrangements, drawing ratio and frictional condition on the forming process were analyzed based on the established models. It showed that the lay-up and thickness of sheets can change the working fluid pressure zone. In their further work [4], suitable process condition to achieve a successful forming of aluminum/steel sheets was predicted by a well-established FE model. The wider working region could be achievable with reduction in thickness of lower strength layer and also when aluminum layer is in contact with drawing punch. In Ref. [5], the effects of key factors on the deep drawing of steel/brass laminated sheets were comprehensively investigated by using numerical and experimental approaches. Results indicated that the layer stacking sequence can significantly affect the final part properties. Karajibani et al. [6] studied the formability of Al-Steel sheets in a deep drawing process through numerical and experimental methods. It was concluded that the drawing ratio of two-layer metallic sheets could be increased by improvement of layer thickness, die arc radius and friction between blank and punch. Analytical and experimental analysis was performed by Dehghani and Salimi [7] to study the formability of copper/stainless steel sheets in deep drawing. It was reported that the thickness variation of stronger layer (stainless-steel) is more uniform than the weaker one (copper). Moreover, the formability of bimetal sheets, in different layer arrangements, in terms of various factors, has the same trends as single-layer sheets.

With the increasing demands for customized components with bimetal materials, it is necessary to develop new forming technology to deal with bimetal composites instead of conventional deep drawing or stamping. Single Point Incremental Forming (SPIF), as an emerging technology, has gone through intensive research over the past decade. During SPIF, localized deformations are superimposed to a sheet by a relatively small tool that follows a predefined path until a final shape is achieved. This unique deformation mechanism brings major benefits, such as better formability, lower forming force, no forming dies and complex equipment needed compared to conventional drawing and stamping processes, making it very suitable for rapid prototyping and low-volume production. Detailed recent developments of SPIF could be found in Refs. [8–10]. Although SPIF has historically been applied mainly to single-layer metal sheets [11–13], in recent years, researchers have started to focus on the shaping of layered metal composite sheets processed by SPIF. Al-Ghamdi et al. [14] investigated the annealing effect on the bond force and formability in the SPIF process of Cu/Steel composite sheets. It was found that the most appropriate annealing temperature for maximizing the formability was 700 °C. Moreover, there was no delamination observed during forming until the maximum angle was achieved. In Ref. [15], annealing was also adopted to reduce the hardening effects and then various characterization tests including formability in stamping and SPIF process were performed. Results revealed that the formability in both of stamping and SPIF increase with the increase of annealing temperature. Furthermore, it was found that formability is limited by delamination in stamping whereas it is not found in SPIF. Using numerical and experimental investigations on the SPIF of Al/Cu two-layer sheets, Honarpisheh et al. [16] demonstrated that by increasing the tool radius and step-down size, the forming force increases and the wall thickness decreases during incremental forming of the studied bimetal materials. Sakhtemanian et al. [17] also studied the effects of layer arrangements of low-carbon steel (St) and pure titanium (Ti) bimetal sheets on SPIF process experimentally and numerically. They concluded that the arrangement of Ti–St shows a higher forming force than St–Ti due to the twinning density of Ti layer in Ti–St mode twice higher than that in St–Ti mode, leading to more work hardening.

According to the literature review, great efforts have been made to investigate the formability of bimetal composite sheets in deep drawing process. Only a few attempts have been made to study the SPIF of bimetal composite sheets, in which, to the best of authors' knowledge, little attention has been paid on the comprehensive study of deformation behaviors during the forming process. Specifically, two main questions should be answered in this research in relation to SPIF of bimetal composite sheets: (i) how do the metal layer arrangement and its properties as well as other parameters comprehensively influence the forming process? (ii) what are the reasons for the different deformation behaviors between monolithic metal sheets and bimetal composite sheets processed by SPIF? It is noted that Cu-Al bimetallic sheets are widely used as conductive, thermal conductive and decoration materials with applications such as contact washer, high and low-voltage power distribution unit (save materials compared to use of Cu only), heat resistant tableware (compared with traditional stainless steel material, its conductivity is much higher and can be more uniformly heated to save energy), decorative panels and so on. In this study, the SPIF of roll-bonded Cu-Al composite sheets has been performed to reveal the deformation behaviors by predictive modeling and experimental approaches to explore the processing ability of this kind of material. The effects of process parameters, such as sheet layer arrangement, step-down size, drawing angle and tool diameter, on formability, surface roughness, thickness variation, as well as forming force are comprehensively analyzed based on experimental results. Furthermore, the derived predictive results through analytical, empirical and numerical approaches are verified with the experimental ones, which shows good agreement with each other.

The rest of this paper is organized as follows. Section 2 introduces the materials and experimental equipment used in this study. Methodology including analytical, empirical and numerical approaches to assess formability, surface roughness, thickness variation and forming force is presented in Section 3. Section 4 presents and discusses the results, illustrating the deformation behaviors in SPIF of Cu-Al

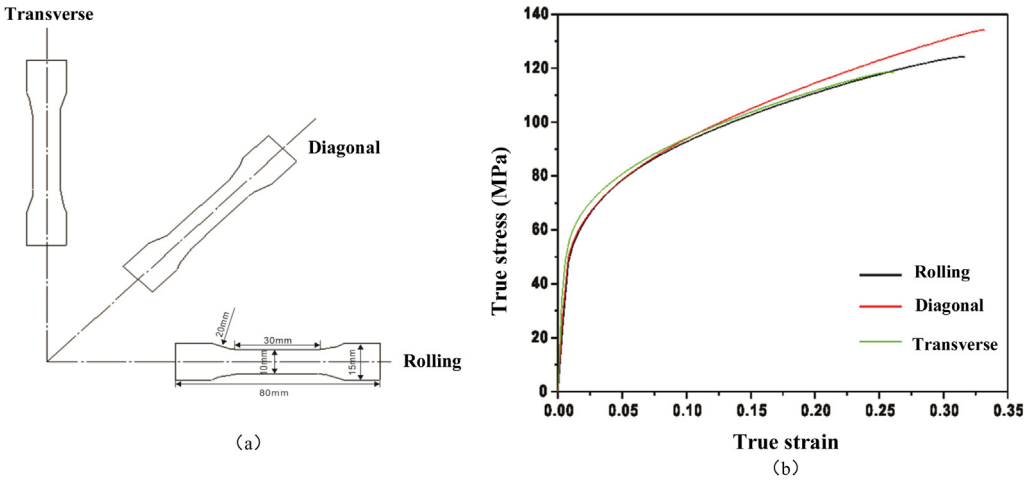

Fig. 1 – Tensile tests: (a) dog-bone shaped samples and (b) true stress–strain curves of Cu-Al composite sheets.

composite sheets. Conclusions are summarized in the last section.

2. Materials and equipment

2.1. *Materials*

In this study, copper (C10100) and aluminum (Al1060-O) composite sheets fabricated by cold roll bonding with an overall thickness of 1 mm were adopted in experiments, which were provided by Luoyang Copper One Metal Material Develops Co., Ltd. The original thicknesses of aluminum-Al1060-O and copper-C10100 sheets were about 8.5 mm and 1.5 mm before rolling. After rolling, the average thicknesses of the aluminum and copper layers were 0.85 mm and 0.15 mm, respectively. Additionally, the bimetal sheet with average aluminum and copper layers of 0.9 mm and 0.1 mm thicknesses as well as single-layer aluminum-Al1060-O and copper-C10100 sheets of 1.0 mm thickness were also provided for experimental comparison purpose. The Cu-Al composite sheets were cut into small pieces with dimensions of 200 mm × 200 mm ready for use. In order to evaluate the mechanical properties of Cu-Al composite sheets, tensile tests with dog-bone shaped samples along rolling, diagonal, and transverse directions (as shown in Fig. 1(a)) were performed in a universal testing machine (Model: DNS-100, manufactured by Sinotest Equipment Co., Ltd.) with a maximum load of 100 kN.

Fig. 2 – Four-axis MIKRON® VCE 800W Pro machine.

During the tensile tests, the strain rate was set to be 5 mm/min. For each sample, three times of tests have been repeated to get average values. The true stress–strain curves were obtained as shown in Fig. 1(b). The anisotropy of tensile properties in three directions are not so obvious, so that in the following FE modeling, they would assume to be isotropic. Mechanical properties for copper, aluminum and their composite are listed in Table 1.

Several papers have presented a view that the mechanical properties of composite sheets are the sum of the proper properties of its component layers. The Young's modulus, Poisson's ratio, Yield stress and Ultimate tensile strength can be calculated by the following equation [18]:

Table 1 – Mechanical properties for copper, aluminum and their composite.

Material	Young's modulus (E) [Gpa]	Poisson's ratio (P)	Yield stress at 0.2% yield (Y) [MPa]	Ultimate tensile strength (UTS) [MPa]
Copper (C10100)	119	0.326	90	200
Aluminum (Al1060-O)	70	0.330	75	110
Cu(0.15 mm)-Al(0.85 mm) bimetal sheet	77	0.330	78	122

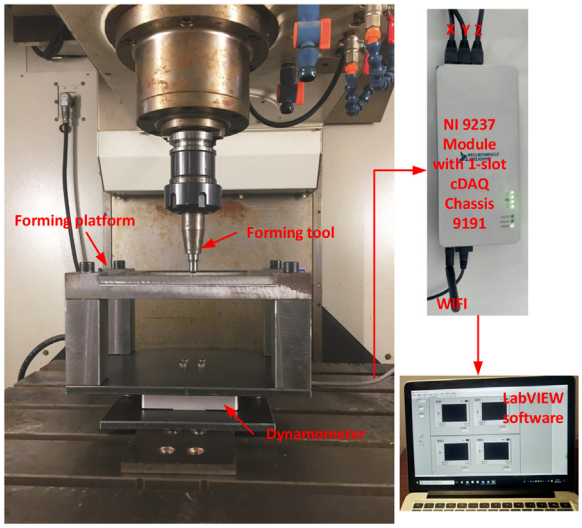

Fig. 3 – Experimental setup with dynamometer.

$$\chi_{Cu\text{-}Al} = c_{Cu}\chi_{Cu} + c_{Al}\chi_{Al} \quad (1)$$

where $\chi_{Cu\text{-}Al}$, χ_{Cu}, and χ_{Al} can refer to Young's modules, Poisson's ratios, Yield stresses and Ultimate tensile strengths. c_{CU} and c_{Al} are the volume (percentage) fractions of metallic components in composite sheet.

The calculated values of E, P, Y, and UTS are 77.4 GPa, 0.329, 77.3 MPa and 123.5 MPa for bimetal composite sheet, which are very close to the values obtained from the tensile tests in Table 1.

2.2. *Experimental equipment*

All the forming tests were performed on a four-axis vertical machining center (MIKRON® VCE 800W Pro), as shown in Fig. 2. Feed rates used in experiments ranged from 1000 mm/min to 4000 mm/min. Tungsten carbide hemispherical tools with different diameters were used to deform Cu-Al composite sheets. The forming tool was fixed not to rotate for all the tests. Before forming, the sheet was clamped on the frame with blank holders. During the forming process, the forming tool was numerically controlled by a Heidenhain iTNC530 controller which follows the specifically designed tool paths. The forming contact zone between forming tool and sheet metal was lubricated by mixture of general lithium-base grease (Brand: EFFICIENT) and mineral oil (Brand: Sinopec SJ10W-40) to reduce friction and avoid excessive wear of the tool surface. The dynamometer used in this study has three channels to measure forces for the x, y and z directions (maximum ranges: x-5000 N, y-5000 N, z-10,000 N) in the experiments. The details of experimental setup with dynamometer system are shown in Fig. 3. Other analysis devices are portable profilometer (Model: TR210) used for surface roughness measurement and optical microscopy (Model: ICX41M, Sunny Optical Technology Co., Ltd.) used for observation of interface morphology.

3. Methodology

In this study, three geometries (groove, truncated cone with variable generatrix and truncated pyramid with fixed drawing angle) were designed to perform experimental investigations. The corresponding designed shapes are represented in Fig. 4. It is noted that groove shape was intended to investigate formability and two-direction (X–Z) forces that could be used to determine the friction coefficient. Truncated cone with variable generatrix was designed to test formability so as to estimate the maximum forming angle based on simple geometric relations. Truncated pyramid with fixed drawing angle was used to investigate surface quality and forming force, as it has flat forming surfaces which could facilitate the surface measurement and force calculation.

3.1. *Formability*

Two geometries (groove and truncated cone with variable generatrix) as shown in Fig. 4(a) and (b), were used to evaluate the process formability of Cu-Al composite sheets. In groove tests, the forming tool follows the zig–zag tool paths to deform the material until the complete crack is observed.

In Fig. 4(b), the maximum formable angle α_{max} can be determined by

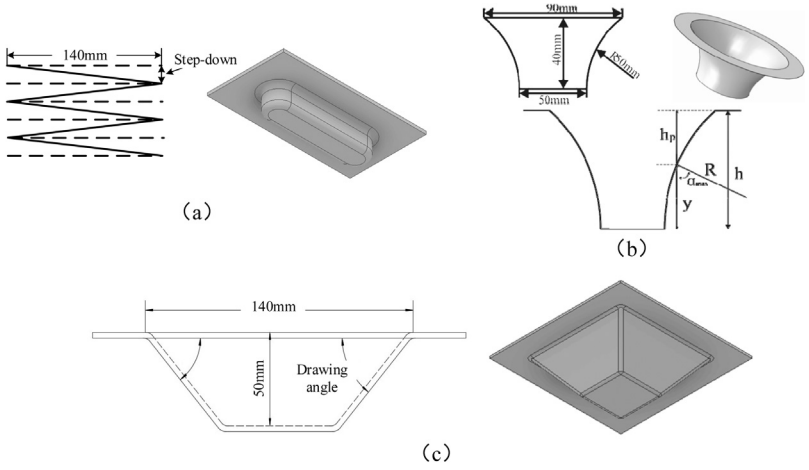

Fig. 4 – Designed geometries: (a) groove, (b) truncated cone with variable generatrix, and (c) truncated pyramid.

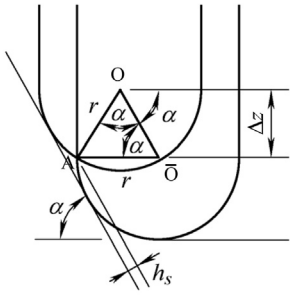

(a) Illustration of scallop height h_s

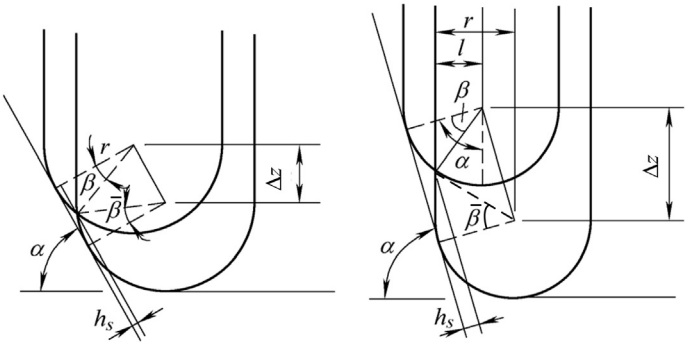

(b) Symmetric zone for scallop height h_s (c) Asymmetric zone for scallop height h_s

Fig. 5 – The geometric relations between scallop height h_s (mm) and process parameters (tool radius r (mm), step-down size Δz (mm), drawing angle α (degree)).

$$\begin{cases} \alpha_{\max} = \arccos\left(\frac{y}{R}\right) \\ y = h - h_p \end{cases} \tag{2}$$

where R is the radius of generatrix; h is the design height; h_p is the crack height.

3.2. *Surface roughness*

Surface roughness has been regarded as a weak point in SPIF process [13]. Surface condition is very complex mainly depending on the tool path (step-down size and tool diameter). In SPIF, surface roughness on the tool-sheet contact surface can be characterized as a resultant of large-scale waviness created by the forming tool path and small-scale roughness induced by large surface strains (see Fig. 1(a) in Ref. [13]). In addition, as the step-down size decreases, the internal tool-sheet contact surface will change from a waviness look to a strict roughness look (see Fig. 2 in Ref. [13]) so that a typical tool-sheet contact surface in SPIF exhibits both roughness and waviness (see Fig. 3 in Ref. [13]). In this study, we investigate scallop height because it is the peak of waviness caused by two adjacent tool paths, which has a direct and significant impact on the surface roughness of SPIF parts that can be approximately measured and characterized by R_z. Therefore, it is of great importance to efficiently predict the surface roughness R_z caused by scallop height given the effects of process parameters, thereby evaluating the surface quality of components. Recently, a simplified analytical model has been proposed to calculate the scallop height [19]. The geometric relations between scallop height and process parameters, such as tool radius, step-down size, and drawing angle are represented in Fig. 5.

In order to establish the model, two situations (I) and (II) should be considered. When the two adjacent tool paths intersect at position A and it satisfies $OA = OA = OO = r$, step-down size Δz can be calculated as

$$\Delta z = r \sin 2\alpha \tag{3}$$

(I) When $\Delta z \le r \sin 2\alpha (\beta = \beta)$ as shown in Fig. 5(b), it derives

$$\sin\beta = \frac{\Delta z}{2r \sin\alpha} \tag{4}$$

$$\cos\beta = 1 - \frac{h_s}{r} \tag{5}$$

Given h_s is far smaller than r, it has

$$h_s = r - \left(r^2 - \frac{\Delta z^2}{4\sin^2\alpha}\right)^{1/2} \tag{6}$$

(II) When $\Delta z > r \sin 2\alpha (\beta \neq \beta)$ as represented in Fig. 5(c), it derives

$$\sin(\alpha - \beta) = \frac{l}{r} \tag{7}$$

$$\cos\beta = 1 - \frac{h_s}{r} \tag{8}$$

$$l = r - \frac{\Delta z}{\tan\alpha} \tag{9}$$

The relation between h_s and Δz can be deduced from Eqs. (7)–(9),

$$h_s = r - r\sin\alpha + \Delta z\cos\alpha - \frac{\cos\alpha}{\tan\alpha}\sqrt{2r\Delta z\tan\alpha - \Delta z^2} \tag{10}$$

It is noted that the tool radius used in SPIF is usually between 5 and 15 mm. The step-down size is chosen smaller than 2 mm. In this case, $\Delta z/r \le 0.4$, α can be estimated using Eq. (3). It derives $\alpha \ge 78^\circ$, which shows that Eq. (10) in (II) is used in the situation with larger drawing angle, step-down size and smaller tool radius.

3.3. Thickness variation

Thickness variation greatly affects the performance of parts formed by SPIF. Sine law is a widely used formula to predict the thickness variation in single-pass SPIF process, which can be expressed as

$$t = t_0\sin(90^\circ - \alpha) \tag{11}$$

where t_0 and t represent the original sheet thickness and deformed sheet thickness; α is the drawing angle.

3.4. Forming force

Forming force is an important process quantity to understand the forming mechanics which has been widely investigated in SPIF [11]. In this study, finite element and empirical models were developed to effectively predict the forming force. Of particular interest, based on the statistical method, Aerens et al. [20] proposed a generalized model to predict the axial force, as depicted in Eq. (12). They claimed that the established formula could be applied to any material based on the tensile strength only.

$$F_z = 0.0716R_m t^{1.57} d^{0.14}\Delta h^{0.09}\alpha\cos\alpha \tag{12}$$

$$\Delta h = \frac{\Delta z^2}{4d\sin^2\alpha} \tag{13}$$

where R_m is the tensile strength (N/mm^2), t is the thickness of the sheet (mm), d is the diameter of the tool (mm), α is the drawing angle (degree), Δh is scallop height, and Δz represents the step-down size (mm).

In order to improve the prediction accuracy for bimetal composite material, the model in Eq. (11) is modified. Given only one thickness of Cu-Al composite sheet used in this study, the initial formula could be set as

$$F_z = ad^b\Delta h^c\alpha\cos\alpha \tag{14}$$

where a, b, and c are coefficients to be determined by experimental data.

3.5. Finite element modeling

A simplified three-dimensional finite element model was developed to simulate the deformation process of Cu-Al composite sheet using ABAQUS software 6.14. An explicit finite-element formulation, instead of the implicit formulation, was used to reduce the required computing time. Specifically, in this FE model, it is assumed that material behavior is isotropic, and a power-law plastic material model was used. The sheet blank with size of 200 mm × 200 mm that consists with the actual experiment, is considered as a deformable body and discretized with shell elements S4R, which are reduced integration elements with one integration point in the plane and five integration points through the thickness. To obtain the proper number of integration points through the thickness and size of elements for meshing the bimetal sheet, preliminary studies were performed and it was found that five integration points through the thickness and shell element size of 1 mm could achieve a proper balance between simulation time and result accuracy. In addition, there are two alternatives to simulate the composite sheet. One is to define a separate section for each sheet layer. The mechanical properties of each sheet layer are attributed to each section. The both sections are tied to each other to simulate the roll-bonded behavior. The other is to define the composite sheet as a whole. As the simulation results show little difference between the two methods in this study, the latter one was adopted to model the composite sheet with improved simulation efficiency. Additionally, the forming tool is modeled using rigid surface elements R3D4 with sizes of 1 mm. The surface-to-surface contact model was used to describe the interaction between the tool and bimetal sheet. The friction behavior between the sheet blank and the forming tool is modeled using the Coulomb friction law with a suitable friction coefficient that will be determined by groove tests.

4. Results and discussion

To investigate the effects of process parameters, including different geometries, step-down size, feed rate, tool diameter and sheet layer arrangements on forming feasibility of Cu-Al composite sheets, series of experiments have been carried out to evaluate the process formability, surface roughness, thickness variation and forming forces. Detailed experimental design is given in Table 2.

4.1. Formability results

In this section, GR and TCG tests were performed to evaluate the influence of layer arrangements, step-down sizes, feed rates and tool diameters on process formability.

4.1.1. Effects of layer arrangements and step-down sizes on formability

For GR tests, the maximum formable depth increases with the increase of step-down sizes from 0.5 mm to 1.5 mm as shown

Table 2 – Experimental design in this study.

Test no.	Geometry	Step-down size (mm)	Feed rate (mm/min)	Tool diameter (mm)	Layer arrangement (up/down)
1-a	GR	0.5	3000	20	Cu/Al(0.15/0.85)
1-b					Al/Cu(0.85/0.15)
2-a	GR	1.0	3000	20	Cu/Al(0.15/0.85)
2-b					Al/Cu(0.85/0.15)
3-a	GR	1.5	3000	20	Cu/Al(0.15/0.85)
3-b					Al/Cu(0.85/0.15)
4-a	TCG	0.2	3000	12	Cu/Al(0.15/0.85)
4-b					Al/Cu(0.85/0.15)
5-a	TCG	0.4	3000	12	Cu/Al(0.15/0.85)
5-b					Al/Cu(0.85/0.15)
6-a	TCG	0.6	3000	12	Cu/Al(0.15/0.85)
6-b					Al/Cu(0.85/0.15)
7-a	TCG	0.8	3000	12	Cu/Al(0.15/0.85)
7-b					Al/Cu(0.85/0.15)
8-a	TCG	0.4	1000	12	Cu/Al(0.15/0.85)
8-b					Al/Cu(0.85/0.15)
9-a	TCG	0.4	2000	12	Cu/Al(0.15/0.85)
9-b					Al/Cu(0.85/0.15)
10-a	TCG	0.4	3000	12	Cu/Al(0.15/0.85)
10-b					Al/Cu(0.85/0.15)
11-a	TCG	0.4	4000	12	Cu/Al(0.15/0.85)
11-b					Al/Cu(0.85/0.15)
12-a	TCG	0.4	3000	7	Cu/Al(0.15/0.85)
12-b					Al/Cu(0.85/0.15)
13-a	TCG	0.4	3000	15	Cu/Al(0.15/0.85)
13-b					Al/Cu(0.85/0.15)
14-a	TCG	0.4	3000	20	Cu/Al(0.15/0.85)
14-b					Al/Cu(0.85/0.15)
15-a	TP (40°)	0.2	3000	12	Cu/Al(0.15/0.85)
15-b					Al/Cu(0.85/0.15)
16-a	TP (40°)	0.4	3000	12	Cu/Al(0.15/0.85)
16-b					Al/Cu(0.85/0.15)
17-a	TP (40°)	0.6	3000	12	Cu/Al(0.15/0.85)
17-b					Al/Cu(0.85/0.15)
18-a	TP (40°)	0.8	3000	12	Cu/Al(0.15/0.85)
18-b					Al/Cu(0.85/0.15)
19-a	TP (30°)	0.4	3000	12	Cu/Al(0.15/0.85)
19-b					Al/Cu(0.85/0.15)
20-a	TP (50°)	0.4	3000	12	Cu/Al(0.15/0.85)
20-b					Al/Cu(0.85/0.15)
21-a	TP (60°)	0.4	3000	12	Cu/Al(0.15/0.85)
21-b					Al/Cu(0.85/0.15)
22-a	TP (40°)	0.4	3000	7	Cu/Al(0.15/0.85)
22-b					Al/Cu(0.85/0.15)
23-a	TP (40°)	0.4	3000	15	Cu/Al(0.15/0.85)
23-b					Al/Cu(0.85/0.15)
24-a	TP (40°)	0.4	3000	20	Cu/Al(0.15/0.85)
24-b					Al/Cu(0.85/0.15)
25	TP (40°)	0.5	3000	10	Al/Cu(0.85/0.15)
26	TP (45°)	0.6	3000	10	Al/Cu(0.85/0.15)
27	TP (45°)	0.5	3000	12	Al/Cu(0.85/0.15)
28	TP (50°)	0.6	3000	12	Al/Cu(0.85/0.15)
29-a	GR	1.0	3000	20	Cu/Al(0.10/0.90)
29-b					Al/Cu(0.90/0.10)
30-a	GR	1.0	3000	20	Cu(1.0)
30-b					Al(1.0)
31	TP (50°)	0.4	3000	12	Al/Cu(0.90/0.10)

Note: GR, TCG, and TC refer to groove, truncated cone with variable generatrix, truncated pyramid with constant drawing angle. Cu/Al means that Cu layer is in contact with forming tool and vice versa.

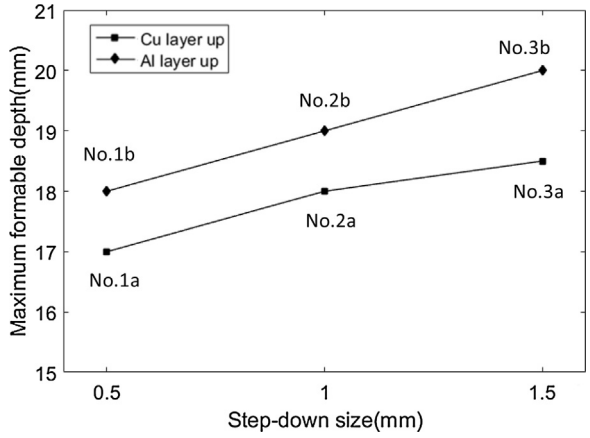

Fig. 6 – The effects of layer arrangements and step-down sizes on maximum formable depth for GR tests.

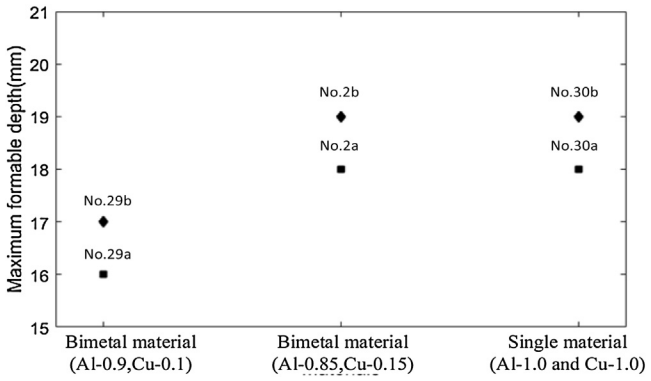

Fig. 8 – The effects of layer arrangements and layer thicknesses on maximum formable depth for GR tests.

in Fig. 6. For the same step-down size, the Al/Cu layer arrangement demonstrates a little bit higher formability than that in the Cu/Al layer arrangement. This phenomenon is further confirmed in TCG tests as presented in Fig. 7. However, in Fig. 7, a decreasing trend for the maximum deformable angle is observed when the step-down sizes increase from 0.2 mm to 0.8 mm. Interestingly, the variation trend of formability between GR and TCG tests is quite opposite. The difference illustrates that formability is actually determined by the interaction of process parameters. For GR tests, a larger tool diameter and step-down size cause the deformation mechanism to include more bending deformation. More materials are stored between two adjacent tool paths to endure further stretching deformation, thus improving the formability. Similar results can be found in Liu et al. [11]. While, for TCG tests, a smaller tool diameter and a larger step-down size cause more stretching deformation leading to the occurrence of fracture. Similar results are also reported in Durante et al. [21] and Shanmuganatan et al. [22].

4.1.2. *Effects of layer arrangements and layer thicknesses on formability*

Fig. 8 shows the effects of layer arrangements and different combinations of layer thicknesses on formability for GR tests. For both bimetal sheets, Al/Cu layer arrangement has higher formability compared with Cu/Al layer arrangement. The thicker Cu layer in bimetal sheets can help enhance the formability. Additionally, the formability of single-layer Al sheet is slightly higher than that of single-layer Cu sheet. Besides, their formability is close to that of bimetal sheet with Cu layer thickness of 0.15 mm.

4.1.3. *Effects of layer arrangements and feed rates on formability*

In Fig. 9, it is observed that the maximum formable angle decreases as the increase of feed rates ranging from 1000 mm/min to 4000 mm/min in TCG tests. The conclusion is consistent with the previous results demonstrated in Hussain et al. [23,24] and Ham et al. [25]. For the same feed rate setting, the formability in Al/Cu layer arrangement is still higher than that in Cu/Al layer arrangement.

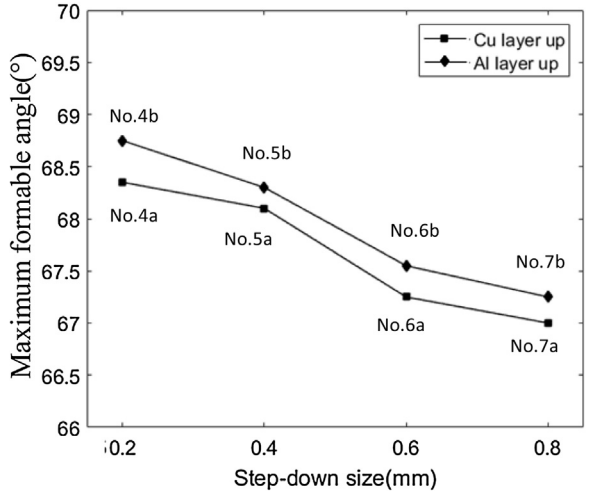

Fig. 7 – The effects of layer arrangements and step-down sizes on maximum formable angle in TCG tests.

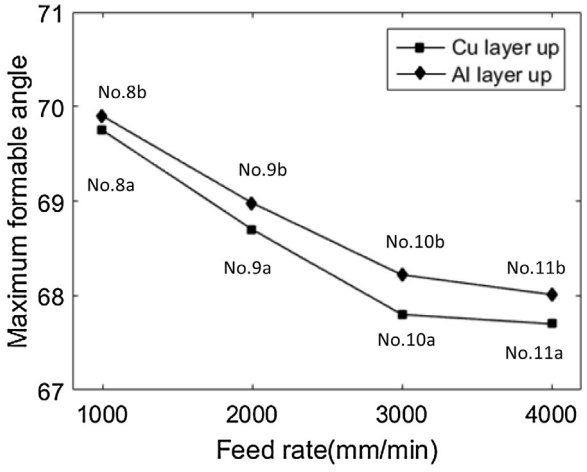

Fig. 9 – The effects of layer arrangements and feed rates on maximum formable angle in TCG tests.

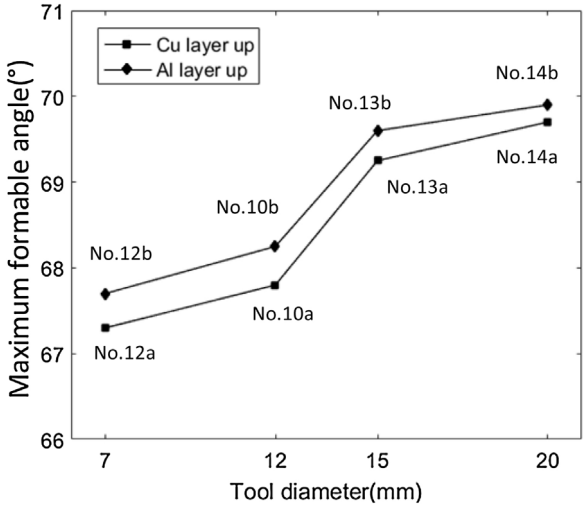

Fig. 10 – The effects of layer arrangements and tool diameters on maximum formable angle in TCG tests.

4.1.4. *Effects of layer arrangements and tool diameters on formability*

As the tool diameter increases from 7 mm to 20 mm, the corresponding maximum formable angle reaches to the highest value of 69.9° in the situation of Al/Cu layer arrangement, as depicted in Fig. 10. Similar to the previous results, the formability in Al/Cu layer arrangement is slightly higher than that in Cu/Al layer arrangement.

4.1.5. *Discussions*

It should be mentioned that, the modes of possible failure in two-layer metal composite sheets processed by SPIF that differ from single-layer sheets could be characterized as follows:

(i) Only one-layer fracture;
(ii) Both two-layers fracture;
(iii) Delamination between two layers.

From the experimental results in this study, the first two modes (i) and (ii) are identified as shown in Fig. 11. In Fig. 11 (a), both Cu and Al layers are cracked while only Cu layer is fractured in Fig. 11(b). It is noted that the above formability results from Sections 4.1.1–4.1.3 were measured when the fracture of both two layers occurred. In the Al/Cu layer arrangement, the crack of Cu layer is always first observed, followed by the crack of Al layer. As asymmetric thicknesses of bimetal composite sheets with different mechanical properties are used, the deformation on the tool-sheet non-contact surface is likely to play a dominant role on the failure mode (i) in the case of Al/Cu layer arrangement with thinner but stronger Cu layer, which possibly further delays the failure mode (ii) with the fracture of thicker but weaker Al layer. However, in the Cu/Al layer arrangement, the crack of thicker but weaker Al layer possibly leads to the crack of thinner but stronger Cu layer simultaneously as the strong bonding strength between two layers. This could explain why the formability of Al/Cu layer arrangement is always higher than that of Cu/Al layer arrangement in this research.

Additionally, interface morphology in Fig. 12 shows that delamination was not be found in the successfully formed parts no matter in Al/Cu layer arrangement or in Cu/Al layer arrangement.

4.2. *Surface roughness results*

In this section, the analysis of surface roughness was performed by comparing the analytical results calculated by Eq. (6) with experimental measured results with different process parameters.

4.2.1. *Effects of layer arrangements and step-down sizes on surface roughness*

The values of surface roughness, R_Z, are reported in Fig. 13. It is shown that the predicted and measured values both increase with the increase of step-down sizes. In addition, the predicted results, except the case with step-down size of 0.2 mm that is close to the measured value, are overestimated compared to the experimental ones. This is possibly because, in the actual forming process, the peak area in the predicted scallop height is usually truncated between adjacent toolpaths, leading to the overprediction.

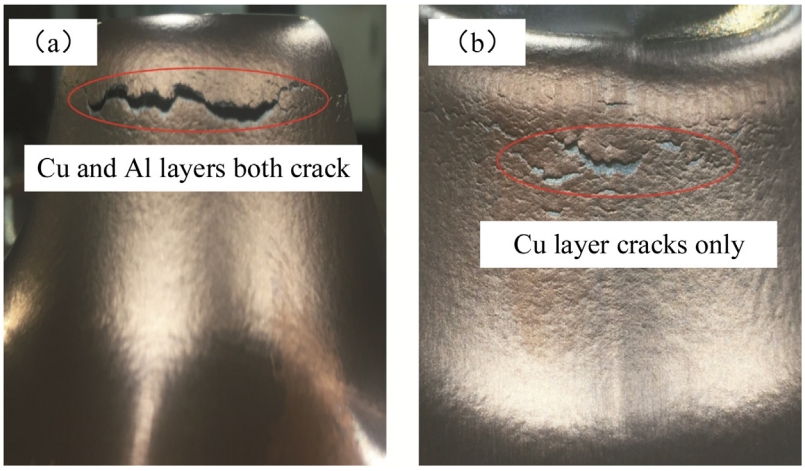

Fig. 11 – Crack morphology in Al/Cu layer arrangement.

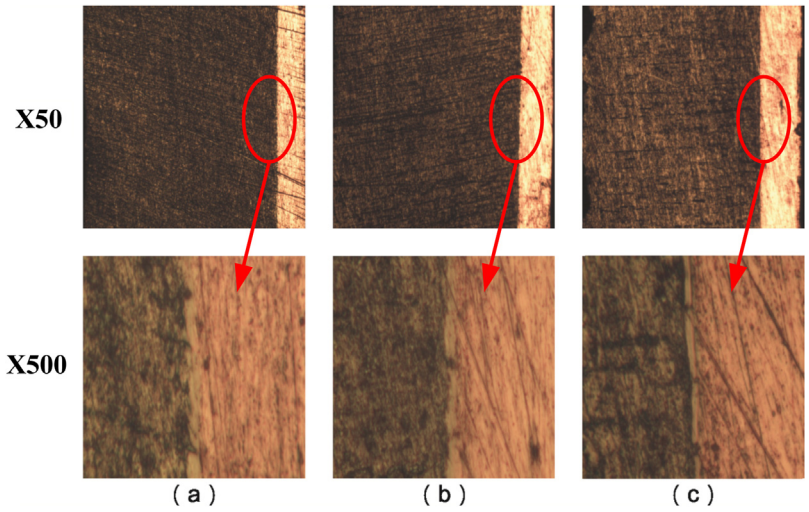

Fig. 12 – Interface morphology: (a) material as received, (b) Al/Cu layer arrangement, and (c) Cu/Al layer arrangement.

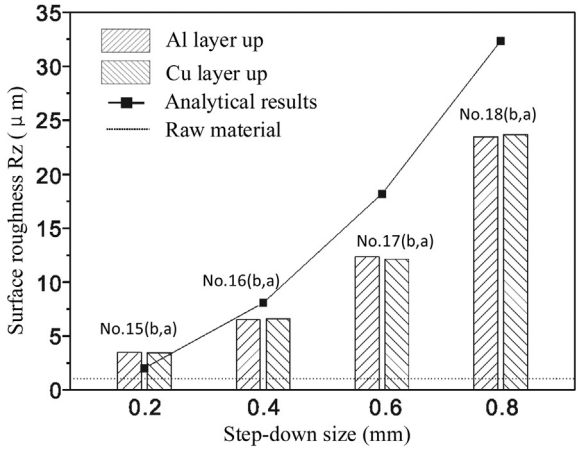

Fig. 13 – Surface roughness R_Z of tool-sheet contact surface with different step-down sizes.

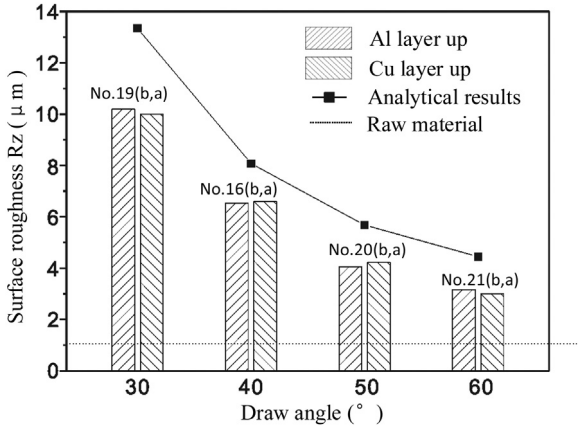

Fig. 14 – Surface roughness R_Z of tool-sheet contact surface with different drawing angles.

For the same step-down size, the surface roughness R_Z between the tool-sheet contact surfaces, Al contact layer and Cu contact layer, has no obvious difference, which demonstrates the surface roughness of tool-sheet contact side is mainly affected by the step-down sizes in this case regardless of the type of materials.

4.2.2. *Effects of layer arrangements and drawing angles on surface roughness*

In Fig. 14, it can be noted that there is a decreasing trend in surface roughness R_Z of tool-sheet contact surface when the drawing angle changes from 30° to 60°. The predicted results overestimate the experimental results to some extent. With the increase of drawing angles, the intervals between two adjacent toolpaths are decreased, leading to smaller surface roughness R_Z. Moreover, layer arrangements in different drawing angles have little influence on the surface roughness R_Z.

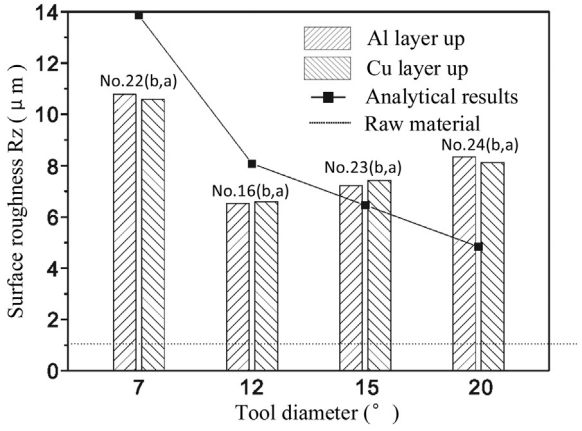

Fig. 15 – Surface roughness R_Z of tool-sheet contact surface with different tool diameters.

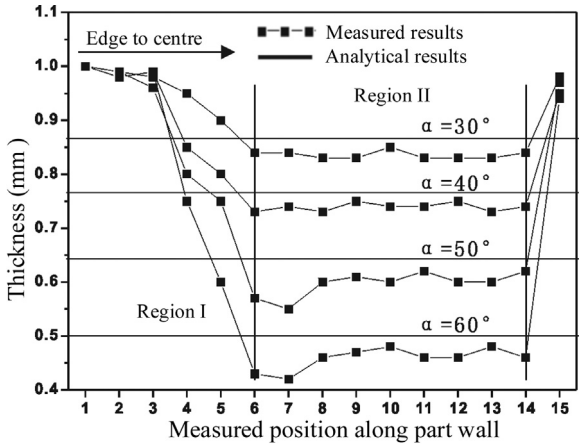

Fig. 16 – Thickness variation of truncated pyramids (TP) with different drawing angles.

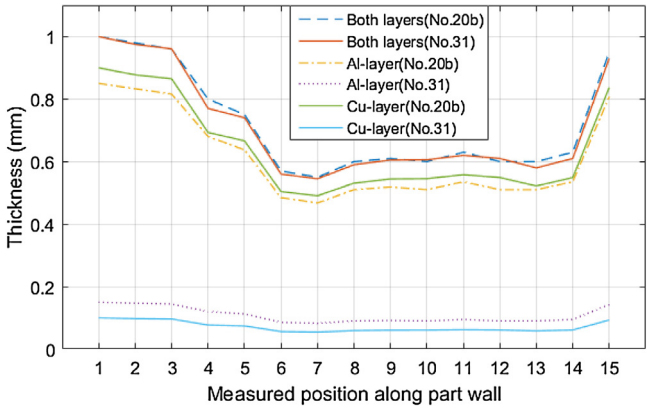

Fig. 18 – Experimental measurements for layer thickness variation of two bimetal materials in the case of TP (50°) and Al/Cu layer arrangement.

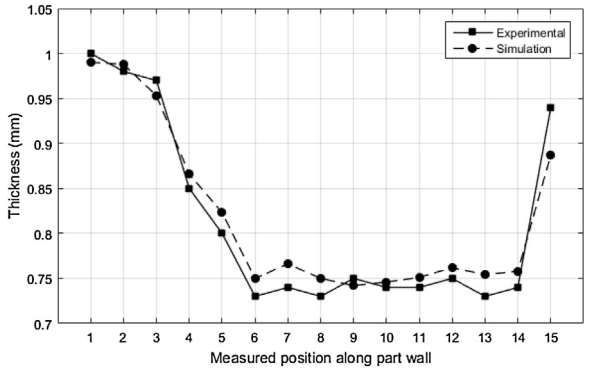

Fig. 17 – Comparison of thickness variation between experimental and FE simulation results in the case of TP (40°).

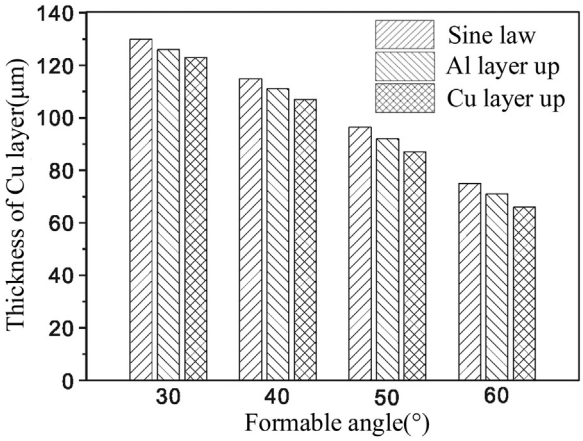

Fig. 19 – Thickness of Cu layer of truncated pyramids (TP) with different drawing angles and layer arrangements.

4.2.3. *Effects of layer arrangements and tool diameters on surface roughness*

In Fig. 15, in the cases of smaller tool diameters (7 mm and 12 mm), the predicted values are higher than the actual measured ones, while the situation is reverse with larger tool diameters. This is because, with the increase of tool diameters, the tool-sheet contact area is also enlarged so that the deformed sheet surface is repeatedly in contact with the forming tool in the subsequent tool paths that easily cause the wear of sheet surface, thereby increasing the surface roughness R_Z.

4.3. *Thickness variation results*

Fig. 16 represents the thickness variation of formed truncated pyramids with drawing angles ranging from 30° to 60°. Two typical regions are divided to analyze the thickness variation.

Region I: Due to the bending effect, the measured thickness is usually larger than the predicted results.

Region II: The measured results are smaller than the predicted ones. This is because the sine law formula is developed based on the shearing deformation only, while in the actual ISF process, the deformation is a combination of shearing, bending and stretching, thereby leading to the overprediction of the actual deformed thickness.

Fig. 17 represents the comparison of thickness variation between experimental and FE simulation results in the case of TP (40°). The FE results are in agreement with the experimental ones. In addition, experimental measurements for layer thickness variation of two bimetal materials with different combinations of layer thicknesses are provided in Fig. 18. It is worth noting that the thicknesses of Cu layer and Al layer in both bimetal sheets vary uniformly along the part wall.

Fig. 19 shows the thickness of Cu layer of truncated pyramids under different drawing angles and layer arrangements. For the same formed geometry, the thickness of Cu layer in Cu/Al layer arrangement is obviously smaller than that in Al/Cu layer arrangement. The phenomenon illustrates that the stronger metal layer (Cu) arranged in the tool-sheet non-contact surface, though it is thinner compared to Al layer in this case, could still have the ability to endure more stretching deformation than that in the contact surface. Furthermore, the

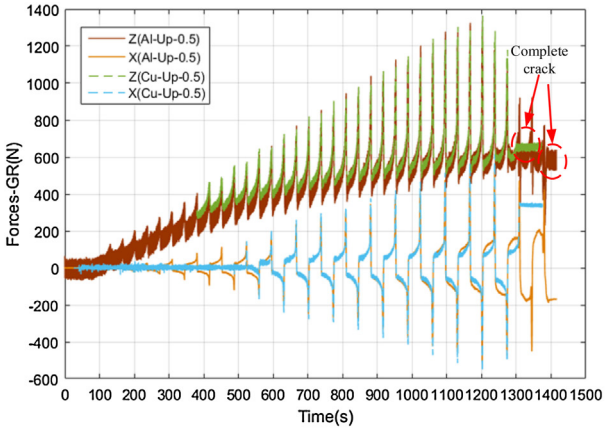

(a) Step-down size: 0.5mm

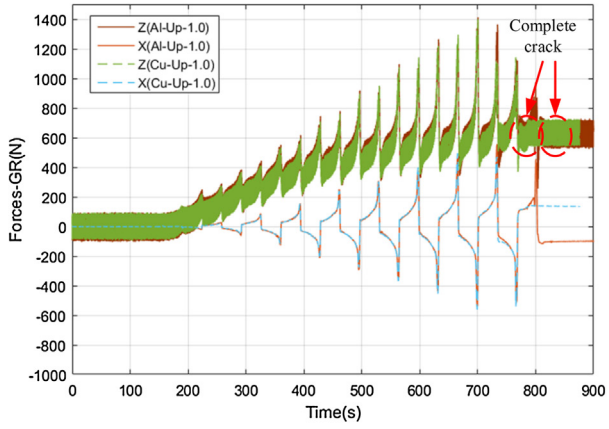

(b) Step-down size: 1.0mm

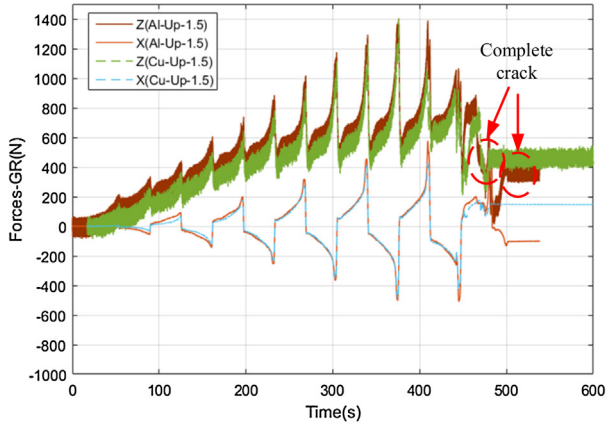

(c) Step-down size: 1.5mm

Fig. 20 – The effects of layer arrangements on forming forces for GR tests with different step-down sizes.

thicker Cu layer can help improve the formability. The above analysis further confirms the previous analysis of formability results. The Al/Cu layer arrangement is likely to delay the crack of both layers.

Table 3 – Friction coefficients obtained from GR tests.

Tool-sheet contact surface	Step-down size (mm)			Average value
	0.5	1.0	1.5	
Cu layer up: μ_f	0.24	0.22	0.23	0.23
Al layer up: μ_f	0.22	0.21	0.27	0.23

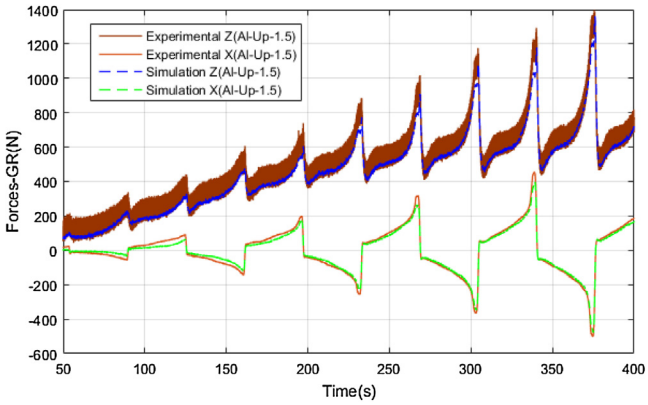

Fig. 21 – Comparison of forming forces between experimental and FE simulation results for GR tests with Al/Cu layer arrangement and step-down size 1.5 mm.

4.4. *Forming force results*

4.4.1. *Effects of layer arrangements and layer thicknesses on forming force*

Fig. 20 shows the effects of sheet layer arrangements on forming forces for GR tests with different step-down sizes. From the results, it can be noticed that there is no big difference for the force variation between Cu/Al layer arrangement and Al/Cu layer arrangement under the same step-down size. The stable and peak value of vertical force (F_Z) in Al/Cu layer arrangement is slightly higher than the situation in Cu/Al layer arrangement. A complete crack could be identified from the force results in all three cases (a–c), which is consistent with the formability results presented in Fig. 6. The force results further illustrate that deformation mode of layer-up sheet in SPIF of bimetal composite sheets is likely to tend to a compression state and that of layer-down sheet tends to a stretching state. This leads to higher formability and larger forming force in Al/Cu layer arrangement compared to Cu/Al layer arrangement, as the exterior thinning but stronger Cu layer could endure more stretching force.

On the other side, the coulomb friction coefficient μ_f between the tool and sheet can be obtained by GR tests using the measured forces F_X and F_Z, which is a widely used method as presented in Ref. [26].

$$\mu_f = \frac{|F_X|}{|F_Z|} \tag{15}$$

The calculated results for friction coefficients are provided in Table 3, which could be applied to the FE simulation. The

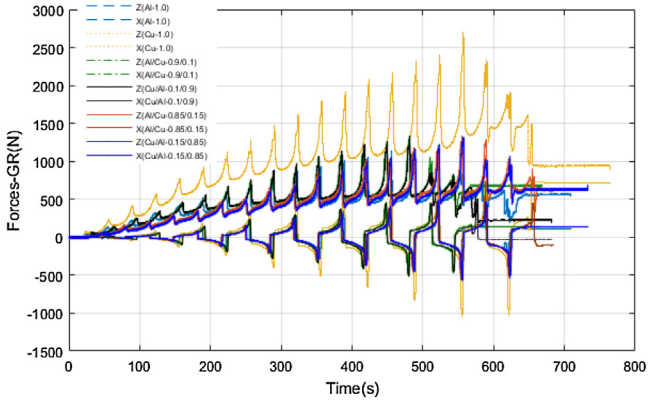

Fig. 22 – Comparison of forming forces in terms of sheets with different layer thicknesses and layer arrangements.

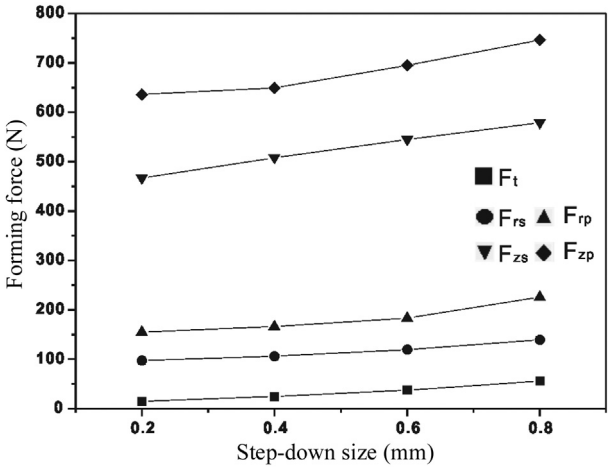

Fig. 24 – The effects of step-down sizes on forming force.

friction coefficients lie between 0.21 and 0.27 in all cases. The average value is very close to each other for both Cu and Al contact layers. Furthermore, FE simulation was carried out to predict the forces of GR tests. Fig. 21 compares the forming forces between experimental and FE simulation results for GR tests with Al/Cu layer arrangement and step-down size of 1.5 mm, which shows that the FE simulation could predict the experimental forces accurately. In Fig. 22, forming forces are compared in terms of sheets with different layer thicknesses and layer arrangements. It is clear that vertical force of bimetal sheets lies between that of single-layer Cu and single-layer Al sheets. As thickness of Cu layer in bimetal sheets increases, the vertical force is getting larger. Besides, for bimetal sheet with Cu layer thickness of 0.1 mm, the stable and peak value of vertical force in Al/Cu layer arrangement is still observed higher than the situation in Cu/Al layer arrangement, which confirms the previous analysis for the case with Cu layer thickness of 0.15 mm.

4.4.2. *Effects of step-down sizes on forming force*

Typical forming forces for TP tests are illustrated in Fig. 23. The vertical (Z) force can be represented by two values: F_{zp} and F_{zs}, in which F_{zp} is the peak vertical force at the step-down point and F_{zs} is the steady vertical force when the tool travels along the z-level tool path. The X(Y) force can be represented by three values: F_t, F_{rs}, and F_{rp}. Here, F_t denotes the tangential force created by friction force that is opposite to tool travel direction. F_{rp} is the steady radial force when the tool travels along the z-level tool path. F_{rp} is the peak radial force at the step-down point. As TP is a symmetric geometry, X force is equal to Y force.

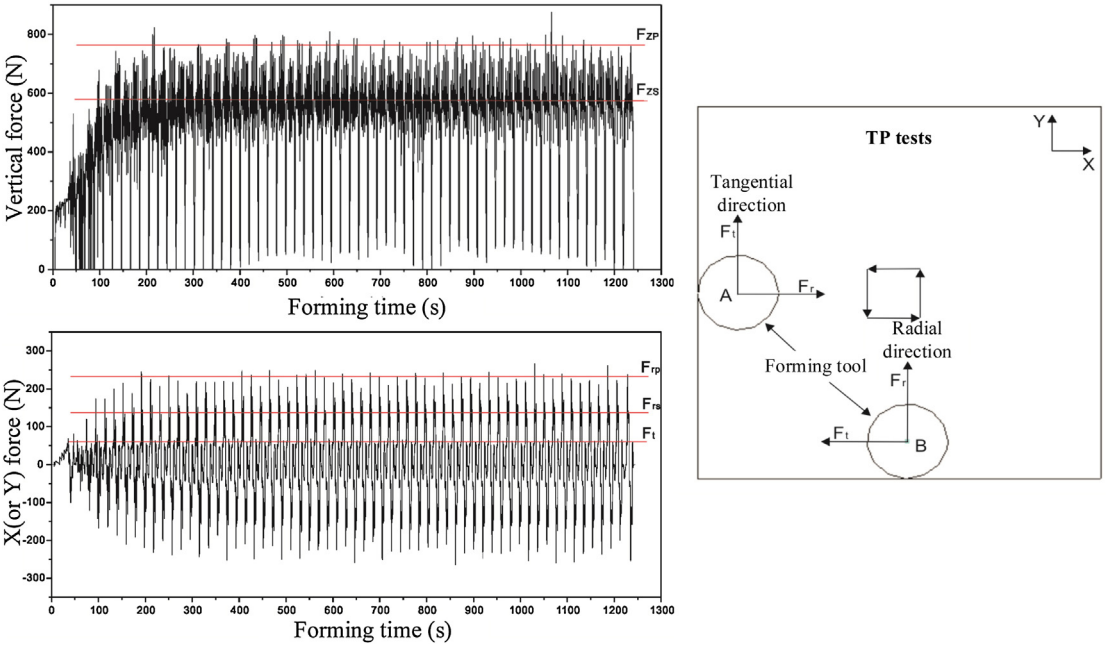

Fig. 23 – Illustration of typical forming forces for TP tests.

Table 4 – Comparison of FE, empirical and experimental F_{zs} forces under different step-down sizes.

Test no.	Experimental force F_{zs} (N)	FE simulation		Empirical formula	
		Predicted force (N)	Error (%)	Predicted force (N)	Error (%)
15-b	466.5	441.6	−5.3	325.0	−30.3
16-b	508.2	495.6	−2.5	368.2	−27.5
17-b	544.9	551.3	1.2	396.1	−27.3
18-b	578.8	583.8	0.9	417.2	−27.9

Table 5 – Comparison of FE, empirical and experimental F_{zs} forces under different drawing angles.

Test no.	Experimental force F_{zs} (N)	FE simulation		Empirical formula	
		Predicted force (N)	Error (%)	Predicted force (N)	Error (%)
19-b	413.2	420.6	1.6	326.7	−20.9
16-b	508.2	523.7	3.0	368.2	−27.5
20-b	553.8	550.3	−0.6	374.2	−32.4
21-b	524.3	494.8	−5.6	341.7	−34.8

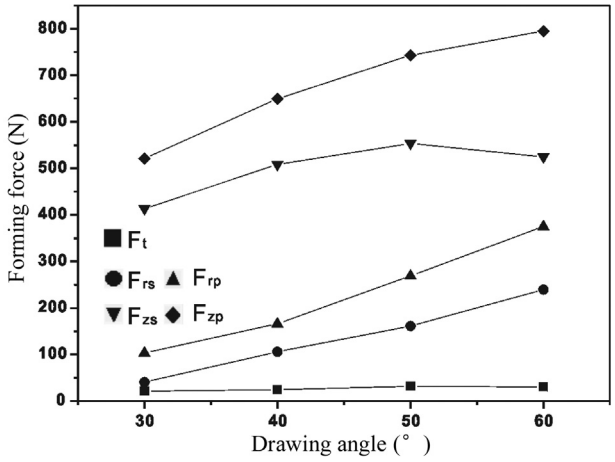

Fig. 25 – The effects of drawing angles on forming force.

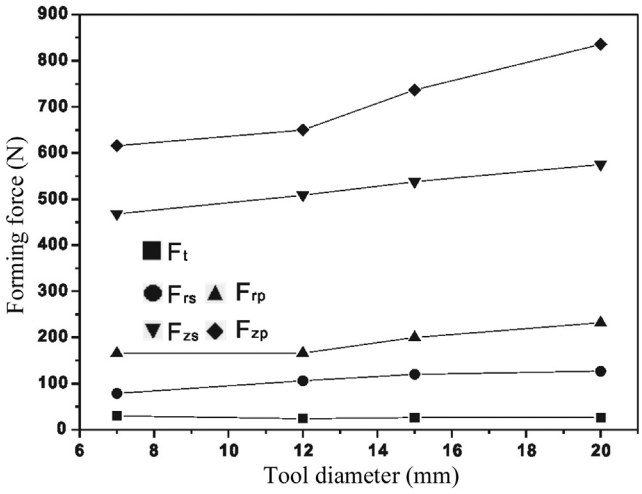

Fig. 26 – The effects of tool diameters on forming force.

In the previous section, force results have shown that there is little difference on the force variation between different metal layer arrangements. In the following research, only Al/Cu layer arrangement was adopted to analyze the forming forces. Results in Fig. 24 shows the effects of different step-down sizes on *X* and *Z* forces. The five components of *X* and *Z* forces are increased as the step-down size increases. However, it is noted that the tangential force (provided by friction force) is the smallest among these five components. Therefore, in most situations, this force component could be neglected in the force modeling. In order to enhance the force predictability, different models (FE and empirical methods) were developed in this study. The corresponding results from these methods are provided in Table 4. The established FE model could predict the steady vertical force accurately with a maximum error of 5.3%. However, the predictive values from empirical model shows a little larger difference compared to the experimental results.

4.4.3. *Effects of drawing angles on forming force*

Fig. 25 shows the effects of different drawing angles on forming force. As presented, the tangential force (F_t) is almost not affected by the drawing angles. While, the radial force (F_{rs} and F_{rp}) obviously increases with the growing of drawing angles. The same situation could be found in the variation of peak vertical force F_{zp}. It should be noted that the steady vertical force F_{zs} reaches to a peak value at the drawing angle of 50° and then decreases. The comparison of FE, empirical and experimental F_{zs} forces under different drawing angles is made as presented in Table 5. The FE results show a good agreement with experimental ones. The predictive errors between the empirical and experimental results are 20.9%, 27.5%, 32.4% and 34.8% corresponding to the drawing angles 30°, 40°, 50° and 60°. Although the predictive errors seem a little large, the empirical values can still reflect the variation trend of F_{zs}.

Table 6 – Comparison of FE, empirical and experimental F_{zs} forces under different tool diameters.

Test no.	Experimental force F_{zs} (N)	FE simulation		Empirical formula	
		Predicted force (N)	Error (%)	Predicted force (N)	Error (%)
22-b	468.0	447.6	−4.4	309.9	−33.8
16-b	508.2	521.4	2.6	368.2	−27.5
23-b	537.8	540.6	0.5	395.5	−26.5
24-b	575.1	567.9	−1.3	433.6	−24.6

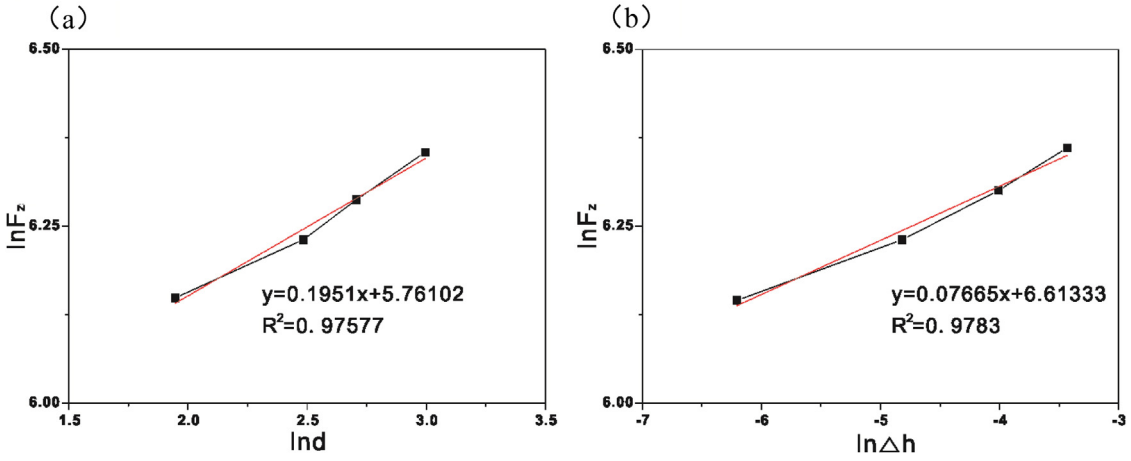

Fig. 27 – Experimental vertical forces for Cu-Al composite sheets in function of (a) tool diameter (log plot, data from tests 16-b, 22-b, 23-b, 24-b) and (b) scallop height (log plot, data from tests 15-b, 16-b, 17-b, 18-b).

Table 7 – Comparison of predicted force derived from modified empirical formula vs. original empirical formula.

Test no.	Experimental force F_{zs} (N)	Modified empirical formula		Original empirical formula	
		Predicted force (N)	Error (%)	Predicted force (N)	Error (%)
25	503.5	526.6	4.6	361.6	−28.2
26	523.4	554.1	5.9	381.4	−27.1
27	576.7	564.9	−1.9	402.5	−30.2
28	545.1	550.6	1.0	391.3	−28.2

4.4.4. *Effects of tool diameters on forming force*

The effects of tool diameters on forming force in TP tests are given in Fig. 26. As shown, except for the tangential force (F_t) that is not sensitive to the variation of tool diameters, the other four force components F_{rs}, F_{rp}, F_{zs} and F_{zp} follow an increasing trend with the increase of tool diameters. The comparison of FE, empirical and experimental F_{zs} forces under different tool diameters is carried out in Table 6 and conclusions similar to those presented in previous sections could be obtained.

4.4.5. *Discussions*

According to the experimental data in all above cases, the vertical peak force F_{zp} is approximately 25–50% higher than the vertical steady force F_{zs}. Additionally, the radial peak force F_{rp} is about 50%-150% larger than the radial steady force F_{rs}, which is greatly influenced by the process parameters.

From the above discussions, the original empirical model for vertical steady force prediction cannot give a satisfactory result. This is because the introduction of Cu-Al composite materials needs new fitting of the model coefficients. The fitting data are shown in Fig. 27. After calculation, the modified empirical model was obtained as

$$F_{zs} = 15.12 d^{0.1951} \Delta h^{0.07665} \alpha \cos\alpha \tag{16}$$

In order to verify the modified empirical model, a new set of experiments have been performed. The predicted F_{zs} derived from modified empirical formula is compared with the ones from the original model as shown in Table 7. It is noticed that the predicted error using the modified model could be significantly reduced to below 5.9% in all cases.

4.5. *Multi-pass forming versus single-pass forming of Cu-Al composite sheets*

In order to further understand the incremental forming mechanics of Cu/Al composite sheets, two multi-pass forming

Table 8 – Design of multi-pass forming strategies.

Target drawing angle	Strategy I		Strategy II	
	First-pass drawing angle	Second-pass drawing angle	First-pass drawing angle	Second-pass drawing angle
50°	30°	20°	40°	10°
60°	30°	30°	50°	10°
70°	30°	40°	60°	10°

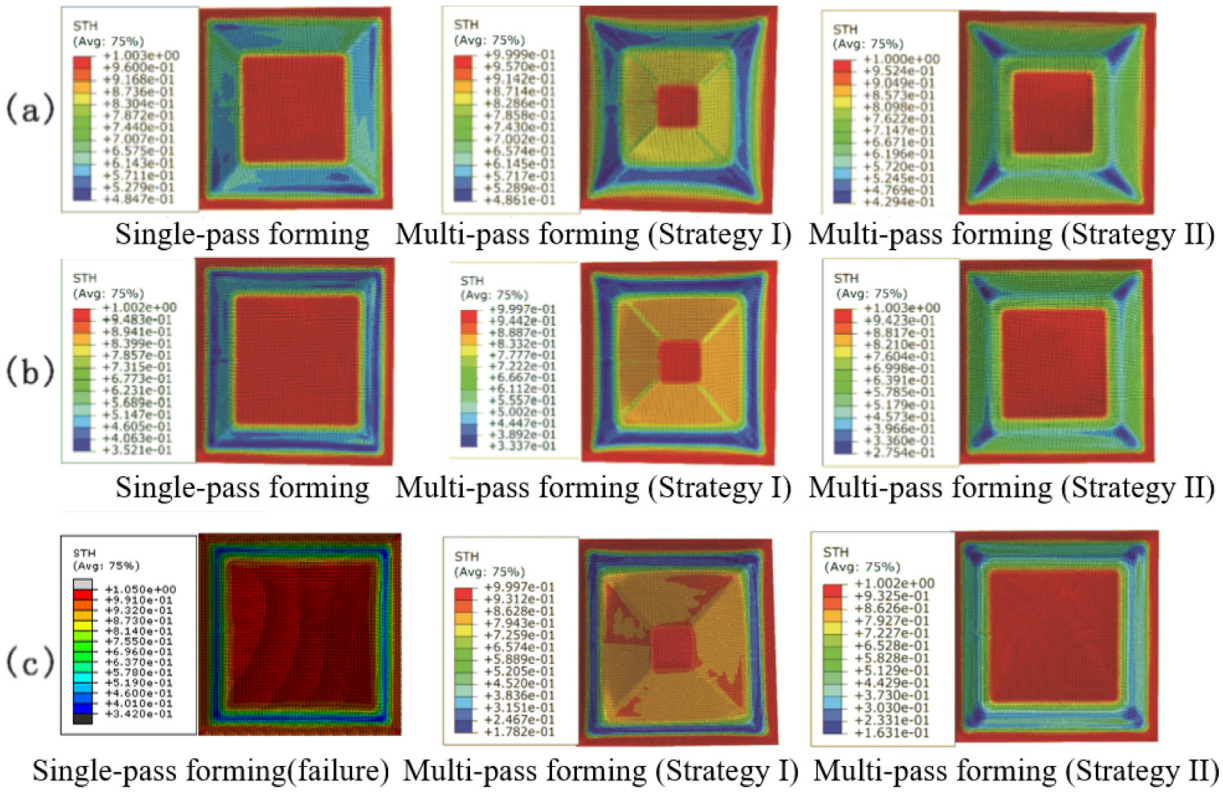

Fig. 28 – Thickness variation of FE simulation: multi-pass forming vs. single-pass forming of TP with drawing angles of 50°, 60° and 70°.

strategies I and II are proposed to manufacture the truncated pyramids with drawing angles of 50°, 60° and 70°. The details are given in Table 8.

The FE results for the thickness variation of formed truncated pyramids with multi-pass forming and single-pass forming are presented in Fig. 28. It is concluded that more uniform thickness variation using multi-pass forming strategy II could be obtained compared to multi-pass forming strategy I and single-pass forming only. However, for the cases with drawing angles of 50° and 60°, thickness variation using single-pass forming is slightly better than that using multi-pass forming strategy I. This illustrates that in the design of multi-pass forming, the interval angle between two adjacent passes should be set to a proper value. Otherwise, the design cannot optimize the thickness variation as well as formability, which may accelerate the forming failure of parts.

The variations of vertical force from FE simulation are shown in Fig. 29. In multi-pass forming strategy I, the steady value of vertical force in pass two is close to that in pass one. However, the force peak value is obviously larger than the value in pass one. In multi-pass forming strategy II, an increasing trend of the steady value of vertical force in pass two could be witnessed, but it is smaller than that in pass one. The peak value follows the same trend as well. When the forming angle between two passes is relative large, the steady value of vertical force in pass two reaches to a peak at the early stage and then decreases to achieve a steady state, as shown in strategy I of Fig. 29(b) and (c). Before the peak value of vertical force, bending deformation could play a dominant role. After the peak value, shearing and stretching are likely to dominate the deformation modes, leading to the reduction of sheet thickness (see strategy I of Fig. 28(a)–(c)) and steady value of vertical force. Finally, when wall thickness reduction induced by shearing and stretching and working hardening during forming achieve a balance, the vertical force stabilizes to a steady level. While, in strategy II, the forming angle between

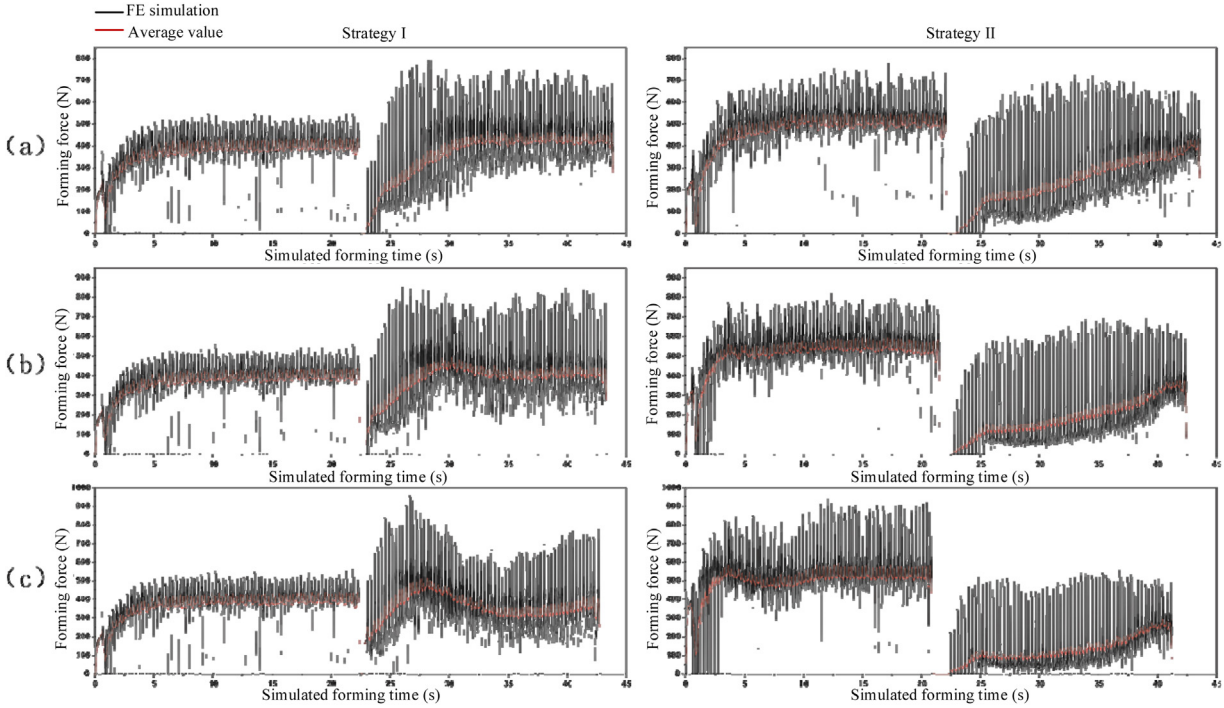

Fig. 29 – Evolution of vertical (Z) force from FE simulation under different drawing angles: (a) 50°, (b) 60° and (c) 70°.

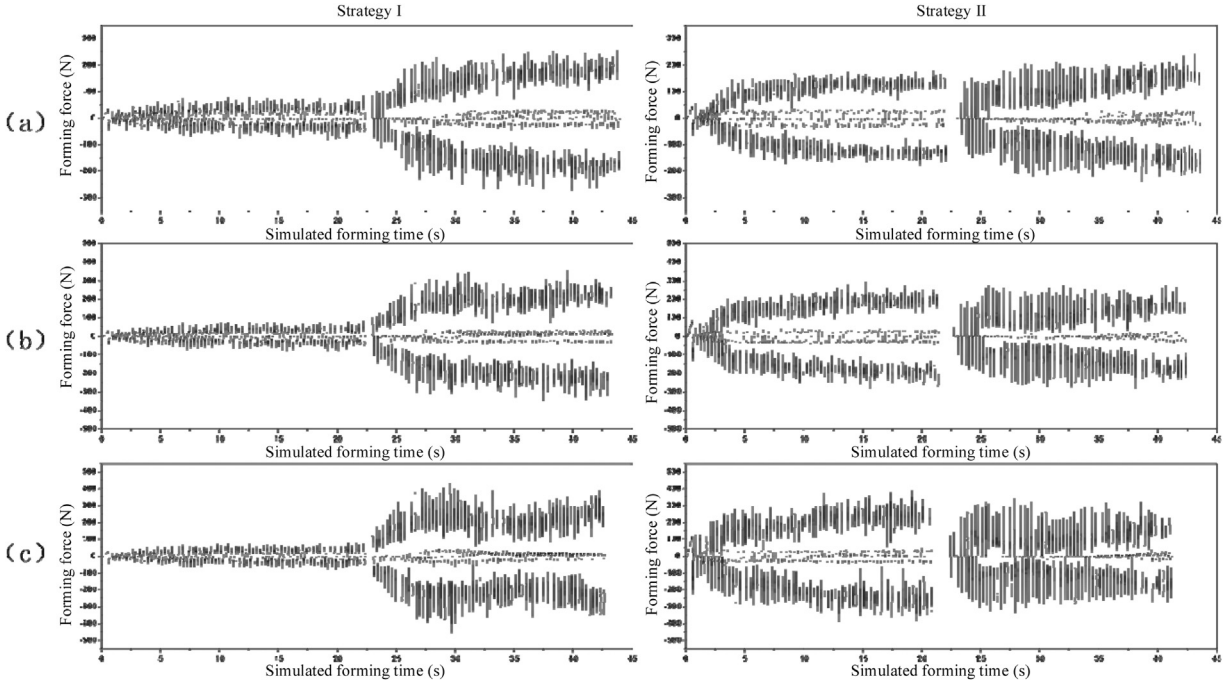

Fig. 30 – Evolution of tangential X(Y) force from FE simulation under different drawing angles: (a) 50°, (b) 60° and (c) 70°.

two passes is relative small, the material of undeformed area in pass one will influence the deformation in pass two, thereby increasing the vertical force of pass two, as presented in strategy II of Fig. 28(a)–(c).

The evolution of tangential X(Y) force from FE simulation under different drawing angles are illustrated in Fig. 30. In strategy I, the X(Y) force, no matter steady value or peak value, is far larger than that in pass one. On the contrary, in strategy II, the steady and peak values of tangential force is slightly smaller than that in pass one. Additionally, the variation trend of tangential force is quite similar in terms of different drawing angles in the same strategy.

Table 9 – FE results of maximum resultant forming force under different forming strategies.

Forming strategies	Maximum resultant forming force (N)		
	Drawing angle (50°)	Drawing angle (60°)	Drawing angle (70°)
Single-pass forming	870	1050	n.a.
Multi-pass forming (Strategy I)	835	965	1128
Multi-pass forming (Strategy II)	777	870	1050

In order to quantify the FE results, the maximum resultant forming force under different forming strategies was calculated and listed in Table 9. From the data, it is noted that compared to the single-pass forming, the multi-pass forming can reduce the resultant forming force to some extent. In addition, the resultant forming force in strategy II is obviously smaller than that in strategy I. It proves that a proper design of multi-pass forming (say, strategy II in this study) can not only facilitate the material flow to improve the thickness variation, but also reduce the forming force.

5. Conclusions

The study in this paper has revealed the deformation behaviors of Cu-Al composite sheets deformed by SPIF regarding the influences of key process parameters. The formability, surface roughness, thickness variation and forming force have been comprehensively investigated by using predictive modeling, FE simulation and experimental analysis to increase the knowledge of processing such kind of bimetal composite material, which reveals that the overall variation of these aspects is quite similar to that of the single-layer material in SPIF. However, different deformation behaviors have been witnessed as well owing to sheet layer arrangements and the corresponding difference of mechanical properties of each layer.

In this context, the research work further clarifies the likely reasons that may lead to the increase of formability and forming force related to the different metal layer arrangements. It is concluded that deformation mode of upper layer sheet tends to a compression state, while that of lower layer sheet tends to a stretching state. The thinner but stronger Cu layer arranged in the exterior side could endure much more stretching force than that arranged in the interior side, thereby delaying the occurrence of fracture. In this sense, main contributions are highlighted from the results presented throughout the paper:

(i) The formability in the Al/Cu layer arrangement in GR and TCG tests is obviously higher than that in the Cu/Al layer arrangement regardless of influences of process parameters, such as step-down sizes, feed rates and tool diameters.
(ii) There is little difference on the surface roughness R_Z of tool-sheet contact surface between two kinds of layer arrangements in TP tests.
(iii) The thickness of residual Cu layer in the Al/Cu layer arrangement is larger than that in the Cu/Al layer arrangement in terms of different formable angles in TP tests.
(iv) Higher forming force in the Al/Cu layer arrangement is observed in GR tests in all cases with different step-down sizes, compared to that of Cu/Al layer arrangement. Moreover, taking Al/Cu layer arrangement for instance, more uniform thickness variation could be achieved in TP tests using proper multi-pass forming strategy compared to single-pass forming only. Also, the overall maximum resultant forming force could be reduced to some extent as well.

Acknowledgements

The authors would like to thank the financial support from the Fundamental Research Funds for the Central Universities (WUT:2017IVA017 and 2017III047) for undertaking this work. Thanks are also given to Mr. Shuaiqi Xing for his assistance of doing additional experiments during revision.

REFERENCES

[1] A.A. Bykov, Bimetal production and applications, Steel Transl. 41 (9) (2011) 778–786.
[2] M.H. Parsa, K. Yamaguchi, N. Takakura, Redrawing analysis of aluminum stainless-steel laminated sheet using FEM simulations and experiments, Int. J. Mech. Sci. 43 (2001) 2331–2347.
[3] S. Bagherzadeh, B. Mollaei Dariani, K. Malekzadeh, Theoretical study on hydromechanical deep drawing process of bimetallic sheets and experimental observations, J. Mater. Process. Technol. 212 (2012) 1840–1849.
[4] S. Bagherzadeh, M.J. Mirnia, B. Mollaei Dariani, Numerical and experimental investigations of hydro-mechanical deep drawing process of laminated aluminum/steel sheets, J. Manuf. Process. 18 (2015) 131–140.
[5] A. Atrian, F. Fereshteh-Saniee, Deep drawing process of steel/brass laminated sheets, Compos. B Eng. 47 (2013) 75–81.
[6] E. Karajibani, A. Fazli, R. Hashemi, Numerical and experimental study of formability in deep drawing of two-layer metallic sheets, Int. J. Adv. Manuf. Technol. 80 (2015) 113–121.
[7] F. Dehghani, M. Salimi, Analytical and experimental analysis of the formability of copper-stainless-steel 304L clad metal sheets in deep drawing, Int. J. Adv. Manuf. Technol. 82 (2016) 163–177.
[8] Y.L. Li, X.X. Chen, Z.B. Liu, J. Sun, F.Y. Li, J.F. Li, G.Q. Zhao, A review on the recent development of incremental sheet-forming process, Int. J. Adv. Manuf. Technol. 92 (2017) 2439–2462.
[9] A.K. Behera, R. Alves de Sousa, G. Ingarao, V. Oleksik, Single point incremental forming: an assessment of the progress

and technology trends from 2005 to 2015, J. Manuf. Process. 27 (2017) 37–62.
[10] J.R. Duflou, A.M. Habraken, J. Cao, R. Malhotra, M. Bambach, D. Adams, H. Vanhove, A. Mohammadi, J. Jeswiet, Single point incremental forming: state-of-the-art and prospects, Int. J. Mater. Form. (2017), http://dx.doi.org/10.1007/s12289-017-1387-y.
[11] Z.B. Liu, Y.L. Li, P.A. Meehan, Experimental investigation of mechanical properties, formability and force measurement for AA7075-O aluminum alloy sheets formed by incremental forming, Int, J. Prec. Eng. Manuf. 14 (11) (2013) 1891–1899.
[12] Z.B. Liu, S. Liu, Y.L. Li, P.A. Meehan, Vertical wall formation and material flow control for incremental sheet forming by revisiting multistage deformation path strategies, Mater. Manuf. Process. 28 (5) (2013) 562–571.
[13] Z.B. Liu, S. Liu, Y.L. Li, P.A. Meehan, Modelling and optimization of surface roughness in incremental sheet forming using a multi-objective function, Mater. Manuf. Process. 29 (2014) 808–818.
[14] K.A. Al-Ghamdi, G. Hussain, R. Hashemi, SPIF of Cu/steel composite sheet: effect of heat treatment on bond force and formability, Mater. Manuf. Process. 31 (6) (2016) 758–763.
[15] K.A. Al-Ghamdi, G. Hussain, On the comparison of formability of roll-bonded steel-Cu composite sheet metal in incremental forming and stamping processes, Int. J. Adv. Manuf. Technol. 87 (2016) 267–278.
[16] M. Honarpisheh, M. Keimasi, I. Alinaghian, Numerical and experimental study on incremental forming of Al/Cu bimetals: influence of process parameters on the forming force, dimensional accuracy and thickness variations, J. Mech. Mater. Struct. 13 (2018) 35–51.
[17] M.R. Sakhtemanian, M. Honarpisheh, S. Amini, Numerical and experimental study on the layer arrangement in the incremental forming process of explosive-welded low-carbon steel/CP-titanium bimetal sheet, Int. J. Adv. Manuf. Technol. 95 (2018) 3781–3796.
[18] R. Uscinowicz, Experimental identification of yield surface of Al-Cu bimetallic sheet, Compos. B Eng. 55 (2013) 96–108.
[19] X.C. Song, B. Lu, J. Chen, Y.L. Wang, Influencing factor analysis on the surface quality of incremental forming parts, J. Mech. Eng. 49 (8) (2013) 84–90.
[20] R. Aerens, P. Eyckens, A. Van Bael, J.R. Duflou, Force prediction for single point incremental forming deduced from experimental and FEM observations, Int. J. Adv. Manuf. Technol. 46 (9–12) (2010) 969–982.
[21] M. Durante, A. Formisano, A. Langella, Observations on the influence of tool-sheet contact conditions on an incremental forming process, J. Mater. Eng. Perform. 20 (6) (2011) 941–946.
[22] S.P. Shanmuganatan, V.S. Senthil Kumar, Metallurgical analysis and finite element modelling for thinning characteristics of profile forming on circular cup, Mater. Des. 44 (2013) 208–215.
[23] G. Hussain, L. Gao, Z.Y. Zhang, Formability evaluation of a pure titanium sheet in the cold incremental forming process, Int. J. Adv. Manuf. Technol. 37 (9–10) (2008) 920–926.
[24] G. Hussain, L. Gao, N. Hayat, N.U. Dar, The formability of annealed and pre-aged AA-2024 sheets in single-point incremental forming, Int. J. Adv. Manuf. Technol. 46 (5–8) (2010) 543–549.
[25] M. Ham, J. Jeswiet, Single point incremental forming and the forming criteria for aa3003, CIRP Ann. Manuf. Technol. 55 (1) (2006) 241–244.
[26] M. Durante, A. Formisano, A. Langella, F. Memola Capece Minutolo, The influence of tool rotation on an incremental forming process, J. Mater. Process. Technol. 209 (9) (2009) 4621–4626.